Supplemental Data

OEP40: a Regulated Glucose-Permeable, ß-Barrel Solute Channel in the Chloroplast Outer Envelope Membrane

Anke Harsman[‡§1], Annette Schock[¶1], Birgit Hemmis[‡], Vanessa Wahl[‡‡], Ingrid Jeshen[¶**], Philipp Bartsch[‡], Armin Schlereth[‡‡], Heidi Pertl-Obermeyer[¶**], Tom Alexander Goetze[¶**], Jürgen Soll[¶**], Katrin Philippar[¶**2], and Richard Wagner[‡§§3]**

Supplemental Methods

Calculating pore size. It is worth to note that even for large channels their conductance is a rather poor measure of the pore size. However, with precautions and in a first approximation the pore size may be calculated according to the Ohmic model of Hille (1). As pointed out by Smart et al. (2), this interpretation is based on the assumption that the pore is a cylindrical conductor having one single characteristic radius. Though, in reality most channel pores have a more complex internal geometry see, e.g., the hourglass-shaped structure of porins (3) and the effective radius of the pore is also determined by the charges of the -and the electric field within the channel pore (4). Nevertheless, a rough correlation between channel pore size and single channel conductance may be deduced with the approach of Smart et al. (2) using the following equation and taking the reduced conductivity of the electrolyte solution within the pore into account (2):

$$d = \frac{\rho \cdot G}{\pi}\left(\frac{\pi}{2} + \sqrt{\frac{\pi}{2} + \frac{4\pi\ell}{\rho G}}\right)$$

in which: d is the diameter of the pore, G is the conductance (325 pS at the lower conductance site, in 250 mM KCl symmetrical solution), ℓ is the length of the constriction zone, assumed to be $\ell_{min} = 0.5\ nm$ to $\ell_{max} = 2\ nm$ (following the model of Hille with a short constriction zone flanked by wide vestibules), and ρ is resistivity of the solution, 49.5 Ω cm at 25°C for a 250 mM KCl solution, but taking into account the correction factor of Smart et al. (2) the value is 247.5 Ωcm.
The resulting diameters based on different length of the restriction zone are listed in the following table:

Table 1: Calculated pore diameter at variable pore length.

restriction zone lenght (ℓ/nm)	pore-diameter (d/nm)
0.5	0.88
1	1.11
1.5	1.28
2	1.43

From high resolution structure combined with MD calculations the effective length of the constriction zone within OmpF has shown to be 2 nm (5).

Calculation of permeability and reversal potential shifts in the OEP40 channel. Changes of the reversal potential after addition of Glucose-1-Phosphate (G1P) and Trehalose-6-Phosphate (T6P):

(1) $$I(E, P_X, z, c_{cis}, c_{trans}) := z^2 \frac{EF^2}{RT} \cdot \frac{(c_{trans} - c_{cis}) \cdot exp\left(\frac{-zFE}{RT}\right)}{1 - exp\left(\frac{-zFE}{RT}\right)}$$ (GHK current equation (1))

(2) $$I_{K^+}(E) = I(E, P_{K^+}, z_{K^+}, c_{K^+cis}, c_{K^+trans})^{[1]}, \quad I_{Cl^-}(E) = I(E, P_{Cl^-}, z_{Cl^-}, c_{Cl^-cis}, c_{Cl^-trans}),$$
$$I_{G1P^-}(E) = I(E, P_{G1P^-}, z_{G1P^-}, c_{G1P^-cis}, c_{G1P^-trans})$$

(3) $$\sum I(E) = I_{K^+}(E) + I_{Cl^-}(E) + I_{G1P^-}$$

[1] Since in OEP40 containing bilayers with 100 mM KCl (cis) and 100 mM NaCl (trans) no zero current shift was observed we can set $P_{K^+} = P_{Na^+}$ and add the concentration of Na^+ ions to obtain the $I_{K^+}(E)$ as total cation current (see Table1 in the manuscript).

Experimental values and parameter values used to fit the GHK-current equation (1) after G1P addition
Parameters:

$P_{K^+} = 4;\ P_{Cl^-} = 1;\ P_{G1P^-} = X$
$z_{Cl^-} = -1;\ c_{Cl^-cis} = c_{Cl^-trans} = 250\ mM$
$z_{K^+} = 1;\ c_{K^+cis} = 262\ mM^*\ c_{K^+trans} = 250\ mM$
$z_{G1P^-} = -1.8;\ c_{G1P^-cis} = 6\ mM;\ c_{G1P^-trans} = 0\ mM$

$V_{rev} = -6.71\ mV$

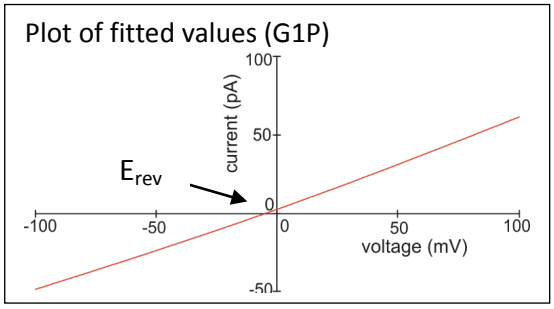

[*] In order to include the counter ions added along with G1P, the respective concentration (i.e. 250mM K^+, 12mM Na^+) was included into the cation concentration on the cis side.

Result:

$$P_{G1P^-} = 48$$

T6P induced shift of V_{rev} in the OEP40 channel
Using the above GHK-approach the T6P induced shift of $V_{rev}\ from\ V_{rev} = 29\ mV\ to\ V_{rev} = 35\ mV$ is compatible with the following parameters

Parameters: $z_{Cl^-} = -1;\ c_{Cl^-cis} \cong 250mM; c_{Cl^-trans} = 20\ mM$
$z_{K^+} = 1;\quad c_{K^+cis} = 251mM^*;\ c_{K^+trans} = 20\ mM$

[*] In order to include the counter ions added along with T6P, the respective concentration was included into the cation concentration on the cis side.

Result:

$$\frac{P_{K^+}}{P_{Cl^-}} = 6:1$$

Supplemental Figures and Table

FIGURE S1. **Amino acid sequence of At-OEP40 and Ps-OEP40 proteins.** Arabidopsis At-OEP40 (At3g57990, 367 amino acids [aa]) is accessible at the ARAMEMNON database (6), the sequence for pea Ps-OEP40 (388 aa) was deposited at NCBI, GenBank acc. no. KT361648. Identical aa (27 %) are shaded in black, similar aa residues in grey. In total, aa identity/similarity is 43%. Oligopeptides sequenced from pea chloroplast OE preparations are indicated by blue lines, predicted ß-sheets and α-helices in At-OEP40 are boxed in magenta and green, respectively (compare Fig. S3). The 10 ß-sheets, which build a potential ß-barrel in At-OEP40 (compare Fig. 1*B*) are numbered, the mainly unstructured C-terminus starts with His^{234} (red arrow).

FIGURE S2. **Production of recombinant Ps-OEP40 protein and α-Ps-OEP40 antiserum.** Numbers indicate molecular mass of proteins in kDa. Arrow heads depict the respective specific protein bands and signals. *A-C*, Purification of rec_Ps-$OEP40^{M19I}$[6His] over-expressed in *E.coli* cells. *A*, Ni-NTA-Sepharose purification as described in Experimental Procedures. 10µl of each protein fraction in urea buffer (50 mM Tris/HCl, pH 8; 100 mM NaCl; 6 M urea, 5mM imidazole) were separated by SDS-PAGE and Coomassie stained. Purification fractions are as follows: FL, flow through of column; W1, W2, wash of column; 100, 200, 500, 1000, elution with 100-1000 mM imidazole in urea buffer. LMW, low molecular weight marker. Asterisks indicate purified Ps-OEP40 protein used for electrophysiological analysis. Please note that rec_Ps-OEP40 protein for generation of antiserum was purified accordingly. *B*, 1µg purified rec_Ps-OEP40 from fractions 100, 1000 in *A* were separated by SDS-PAGE and subjected to immunoblot analysis using an antibody directed against the C-terminal His tag of the protein (Anti-His_6, Roche LifeScience). *C*, 10 ng of Ni-NTA purified Ps-OEP40 protein (pP, compare *A*) as well as 8 µg each of pea chloroplast outer envelope (OE) and inner envelope (IE) proteins were separated by SDS-PAGE and subjected to immunoblot analysis using an antiserum directed against the rec_Ps-OEP40 protein (α-PsOEP40). Please note that both antisera in *B* and *C* detect single specific bands for the rec_Ps-OEP40 protein at 43 kDa, which exactly correspond to the specific signal of the native Ps-OEP40 in chloroplast OE membranes (compare Figs. S2*C, F* with Fig. 1*A*). *D, E*, Generation and purification of rec_Ps-$OEP40^{M19I}$[6His] in cell free systems (mock control samples for electrophysiology). *D*, *In vitro* translation of Ps-$OEP40^{M19I}$/pET21d with the TNT System was performed as described in Experimental procedures. For control, translation reactions without (-) and with (+) the Ps-OEP40 plasmid construct were performed in the presence of radiolabeled ^{35}S-Met/Cys. *Left,* 1 µl of each reaction was separated by SDS-PAGE and label incorporation was monitored by autoradiography. *Right,* 5 µl of each reaction were separated by SDS-PAGE and subjected to immunoblot analysis with α-Ps-OEP40 (see *C*). *E*, *In vitro* translation of Ps-$OEP40^{M19I}$/pET21d with the plant wheat germ lysate (see Experimental Procedures). Respective samples were separated by SDS-PAGE and subjected to immunoblot analysis with α-PsOEP40 (see *C*). *Left,* 5 µl of non-purified translation product (TP) and 5 µl of *in vitro* translated, Ni-NTA purified and concentrated Ps-OEP40 (pP). *Right,* 5 µl of *in vitro* translated, Ni-NTA purified and concentrated Ps-OEP40 (pP) as well as excised protein bands (#1: Ps-OEP40, #2: control gel slice) after a second purification step via SDS-PAGE (see Experimental Procedures for detail). Asterisks indicate respective non-labeled samples used in planar lipid bilayer measurements. Please note that the α-PS-OEP40 antiserum detects a single, specific protein band at 43 kDa (compare with *C*). *F*, Immunoblot analysis of Ps-OEP40 in chloroplast subfractions and mitochondria. Please note that the blot for Ps-OEP40 shown in Fig. 1*A*, upper panel corresponds to a section in the first four lanes of the depicted entire gel blot. Equal protein amounts (5µg) of pea chloroplast outer envelope (OE), inner envelope (IE), stroma (str), thylakoids (thy), and isolated pea mitochondria were separated by SDS-PAGE and subjected to immunoblot analysis using antibodies directed against recombinant Ps-OEP40 (α-Ps-OEP40). *Right,* the antisera α-TOM40 (7), α-Tic110 (8), α-PsbB (Agrisera), and α-LSU (see Fig. 1*A*) were used as controls for mitochondria (Mit, 5µg protein), IE (10µg protein), thy (15µg protein), and str (5µg protein), respectively. Mitochondria were isolated according to (9).

FIGURE S3. **OEP40 is a transmembrane protein with high ß-sheet content.** *A,* After treatment with either 1 M NaCl, 0.1 M Na_2CO_3 (pH 11.3), 4 M urea, or 1 % Triton X-100, pea OE membranes (20 µg protein for each assay) were separated into insoluble (P) and soluble protein (S) fractions by ultracentrifugation, separated via SDS-PAGE and analyzed by immunoblotting with antisera directed against Ps-OEP40 and Ps-OEP37. *B,* Circular dichroism (CD) spectra for At-OEP40 and At-OEP37 proteins. Red (At-OEP40) and blue (AtOEP37) lines represent averaged sample spectra (n = 10, averaged baseline spectra subtracted) of consecutive scans from 190-260 nm. Percentage of alpha-helical, ß-sheet, turn and unordered secondary structures in At-OEP40 and At-OEP37 proteins are indicated below. Spectra were analyzed by the DICHROWEB analysis webserver (10). Data represent mean values from SELCON3, CONTIN, and CDSSTR programs. *C*, Bioinformatic analysis of the putative OEP40 topology and structure. Sequence based structure prediction and modeling of putative OEP40 tertiary structure from Arabidopsis (UniProtKB: Q9M2P9). The amino acid sequence with predicted secondary structure is depicted by colored bars. The relative height of the bars is defined by consistent structure prediction of different prediction servers and algorithms [PSIPRED (11), Scratch Protein Predictor, SPP (12), PRED-TMBB (13), TMBpro, I-TASSER (14)]. Beta-sheets and alpha-helices used to construct a possible tertiary structure shown in Fig. 1*B* are framed and underlined, respectively.

FIGURE S4. **Dependence of the interevent dwell times on the glucose concentration.** The interevent dwell times, denoting the time interval between two slow glucose blocking events, were analysed for three independent single channel recordings at V_m = -80 mV and four different glucose concentrations. The depicted values were obtained from the corresponding mean variance analysis by an exponential fit of the interevent dwell time histogram. The slope in the regression corresponds to the second order $k_{on} \cong 8.58 \pm 1.15 \cdot 10^{-3} M^{-1} s^{-1}$ rate of glucose to the cannel vestibule (15).

FIGURE S5. **Effect of maltose on single channel activity of reconstituted OEP40.** *A*, *B,* Single channel recordings in symmetrical buffer conditions in absence (*A*) and presence of 2 mM maltose in *cis*/*trans* (*B*). The indicated voltage amplitude (V_m) was applied. *C,* Current-voltage ramp (-80 mV to 80 mV, sweep-rate 15 mV/s) of a single open OEP40 channel in symmetrical buffer. *D,* Current-voltage ramp (-100mV to 100 mV, sweep-rate 15 mV/s) of a single open OEP40 channel in the presence of 2 mM maltose (cis/trans) under symmetrical buffer conditions.

FIGURE S6. **Occupation of subconductance states of OEP40 changes in the presence of T6P.** Summary of the dwell time analysis from three independent single channel recordings at V_m = ±80 mV (top and bottom, respectively) in the absence and presence of 1 mM T6P (cis/trans) depicting the relative occupation of the fully open, closed and subconductant state.

FIGURE S7. **Mutation of *OEP40* in Arabidopsis.** *A,* Schematic representation of the *At-OEP40* gene (At3g57990). The black arrow indicates the single exon. Two T-DNA insertion sites in the promoter region (*oep40-1*, position -21) and in the exon (*oep40-3*, position +245) are indicated by triangles. T-DNA is pCSA110 in both lines: SAIL_266_D10 (*oep40-1*) and SAIL_759_A01 (*oep40-3*). Binding sites for *FAX1* gene specific primers and T-DNA specific left border (LB) primers used for PCR genotyping and for RT-PCR are depicted (Table S1). +1: predicted transcriptional start. *B, OEP40* transcript content (relative units) in 14-day-old seedlings of Col-0 wild-type and homozygous *oep40-1*, *oep40-3* lines. RNA was reverse transcribed into cDNA and qRT-PCR was performed as described (16). The transcript content was quantified relative to 1000 actin 2/8 mRNA molecules (n = 3 ± SD). For primer positions, see *A*, for sequences Table S1. *C,* Immunoblot of At-OEP40 on total membrane protein extracts (110 µg each) isolated from rosette leaves of mature of Col-0 wild-type and homozygous *oep40-1*, *oep40-3* lines. Specific antiserum was directed against At-OEP40, staining of the blotting membrane with amido black (a.b.) was used as loading control. Numbers indicate the molecular mass of proteins in kDa. Please note that the absence of a signal in the *oep40-3* knockout demonstrates the specificity of the antiserum directed against At-OEP40 (compare with Fig. S2 for Ps-OEP40).

FIGURE S8. **Expression of *At-OEP40* during plant development and the shoot apical meristem.** Data was provided at the Arabidopsis eGFP browser website at bar.uturonto.ca (17). *A,* AtGenExpress developmental atlas (18). *B,* Expression of *At-OEP40, At-LFY* (AT5g61850, transcription factor for floral meristem identity, see Fig. 6), and *At-TPS1* [At1g78580, T6P synthase, compare (19)] in the Arabidopsis shoot apical mersitem (SAM) stem cell niche (20). In *Arabidopsis,* the SAM consists of 35 stem cells, located within the central zone (CZ). Stem cells are surrounded by several million differentiating cells that are part of the adjacent peripheral zone (PZ) and developing organs. The cells of the Rib-meristem (RM) that are located just beneath the CZ provide positional cues necessary for stem cell maintenance (20). Cell protoplasts were sampled by fluorescence-activated cell sorting, according to 3 marker genes [see (20) for details]. Please note that data in *A* and *B* have been generated in independent experimental setups and thus, although normalized by the same parameters (i.e. GCOS, TGT=100, see eGFP browser website), are not directly comparable. In total shoot apex tissue *(A)*, RNA levels of At-*OEP40* (~ 140) as well as At-*LFY* (~ 290) and At-*TPS1* (~ 240, see eGFP browser website) are not significantly elevated. Relation of At-*OEP40* transcript content to At-*LFY,* At-*TPS1* in *(B)*, however indicates a site of peak expression in RM cells.

TABLE S1. Oligonucleotides used in this study

PCR genotyping	
At-OEP40-1_fw	5'-GGGATAAACAAACAACCAGGC-3'
At-OEP40-1_rv	5'-TATCCACCACCTCAATCGAAG-3'
At-OEP40-3_fw	5'-TTTCGTGAAGAGCAAAAGCC-3'
LB1 SAIL	5'-GCCTTTTCAGAAATGGATAAATAGCCTTGCTTCC
Quantitative real time RT-PCR	
Act2/8 fw	5'-GGTGATGGTGTGTCT-3'
Act2/8 rv	5'-ACTGAGCACAATGTTAC-3'
At-OEP40_LC_fw	5'-CGTTAGGGTTCCTACGG-3'
At-OEP40_LC_rv	5'-CTCAGCTACATTGCCCTC-3'
Isolation of Ps-OEP40 cDNA	
Ps-noep40fw	5'-ATGAAGCTCTCCCTCAAATTCCACAAC-3'
Ps-noep40revB	5'-AAACTTGTTCTCCCCTTATTGCTTGC-3'
Site-directed mutagenesis of Ps-OEP40 cDNA	
Ps-OEP40_PM1_M2_fw	5'-CAAACCCAAATAATCACAGCAAAACTACCAATCACC-3'
Ps-OEP40_PM2_M2_rv	5'-GGTGATTGGTAGTTTTGCTGTGATTATTTGGGTTTG-3'
Subcloning of OEP40 cDNAs into pET21d	
At-OEP40_fl_fw(NcoI)	5'-CCATGGATGAAGGCATCGATGAAGT-3'
At-OEP40_fl_+st_rv(XhoI)	5'-CTCGAGTCAAGCAGCTCCTTTCAAAG-3'
At-OEP40_fl_-st_rv(XhoI)	5'-CTCGAGAGCAGCTCCTTTCAAAGCTT-3'
Ps-noep40ps_NcoI	5'-GGCCATGGCCATGAAGCTCTCCCTCAAATTCCAC-3'
Ps-noep40ps_XhoI	5'-TGCTCGAGGGAAGAAGAAGCAGCAGTGGCA-3'

References

1. Hille, B. (2001) *Ionic Channels of Excitable Membranes*, Sinauer Ass. Inc., Sunderland, Ma 01375
2. Smart, O. S., Breed, J., Smith, G. R., and Sansom, M. S. P. (1997) A novel method for structure-based prediction of ion channel conductance properties. *Biophys. J.* **72**, 1109-1126
3. Cowan, S. W., Schirmer, T., Rummel, G., Steiert, M., Ghosh, R., Pauptit, R. A., Jansonius, J. N., and Rosenbusch, J. P. (1992) Crystal structures explain functional properties of two E. coli porins. *Nature* **358**, 727-733
4. Eisenberg, R. S. (1996) Computing the field in proteins and channels. *J. Membr. Biol.* **150**, 1-25
5. Im, W., and Roux, B. t. (2002) Ions and Counterions in a Biological Channel: A Molecular Dynamics Simulation of OmpF Porin from Escherichia coli in an Explicit Membrane with 1M KCl Aqueous Salt Solution. *J. Mol. Biol.* **319**, 1177-1197
6. Schwacke, R., Schneider, A., van der Graaff, E., Fischer, K., Catoni, E., Desimone, M., Frommer, W. B., Flügge, U. I., and Kunze, R. (2003) ARAMEMNON, a novel database for Arabidopsis integral membrane proteins. *Plant Physiol.* **131**, 16-26
7. Carrie, C., Kuhn, K., Murcha, M. W., Duncan, O., Small, I. D., O'Toole, N., and Whelan, J. (2009) Approaches to defining dual-targeted proteins in Arabidopsis. *Plant J.* **57**, 1128-1139
8. Lübeck, J., Soll, J., Akita, M., Nielsen, E., and Keegstra, K. (1996) Topology of IEP110, a component of the chloroplastic protein import machinery present in the inner envelope membrane. *EMBO J.* **15**, 4230-4238
9. Whelan, J., Knorpp, C., and Glaser, E. (1990) Sorting of precursor proteins between isolated spinach leaf mitochondria and chloroplasts. *Plant Mol. Biol.* **14**, 977-982
10. Whitmore, L., and Wallace, B. A. (2008) Protein secondary structure analyses from circular dichroism spectroscopy: methods and reference databases. *Biopolymers* **89**, 392-400
11. Buchan, D. W., Minneci, F., Nugent, T. C., Bryson, K., and Jones, D. T. (2013) Scalable web services for the PSIPRED Protein Analysis Workbench. *Nuc. Acids Res.* **41**, W349-357
12. Cheng, J., Randall, A. Z., Sweredoski, M. J., and Baldi, P. (2005) SCRATCH: a protein structure and structural feature prediction server. *Nuc. Acids Res.* **33**, W72-76
13. Bagos, P. G., Liakopoulos, T. D., Spyropoulos, I. C., and Hamodrakas, S. J. (2004) PRED-TMBB: a web server for predicting the topology of beta-barrel outer membrane proteins. *Nuc. Acids Res.* **32**, W400-404
14. Zhang, Y. (2008) I-TASSER server for protein 3D structure prediction. *BMC Bioinformatics* **9**, 40
15. Movileanu, L. (2009) Interrogating single proteins through nanopores: challenges and opportunities. *Trends Biotechnol.* **27**, 333-341
16. Duy, D., Wanner, G., Meda, A. R., von Wiren, N., Soll, J., and Philippar, K. (2007) PIC1, an ancient permease in Arabidopsis chloroplasts, mediates iron transport. *Plant Cell* **19**, 986-1006
17. Winter, D., Vinegar, B., Nahal, H., Ammar, R., Wilson, G. V., and Provart, N. J. (2007) An "Electronic Fluorescent Pictograph" Browser for Exploring and Analyzing Large-Scale Biological Data Sets. *PLoS ONE* **2**, e718
18. Schmid, M., Davison, T. S., Henz, S. R., Pape, U. J., Demar, M., Vingron, M., Scholkopf, B., Weigel, D., and Lohmann, J. U. (2005) A gene expression map of Arabidopsis thaliana development. *Nat. Genet.* **37**, 501-506
19. Wahl, V., Ponnu, J., Schlereth, A., Arrivault, S., Langenecker, T., Franke, A., Feil, R., Lunn, J. E., Stitt, M., and Schmid, M. (2013) Regulation of flowering by trehalose-6-phosphate signaling in Arabidopsis thaliana. *Science* **339**, 704-707
20. Yadav, R. K., Girke, T., Pasala, S., Xie, M., and Reddy, G. V. (2009) Gene expression map of the Arabidopsis shoot apical meristem stem cell niche. *Proc. Natl. Acad. Sci. U.S.A.* **106**, 4941-4946

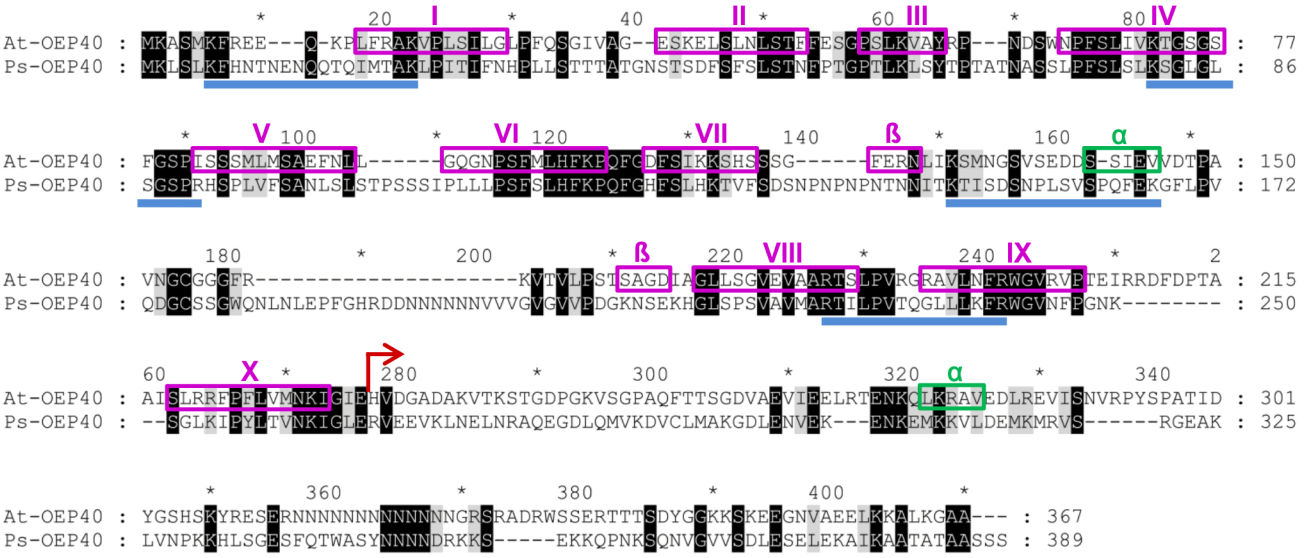

Figure S1

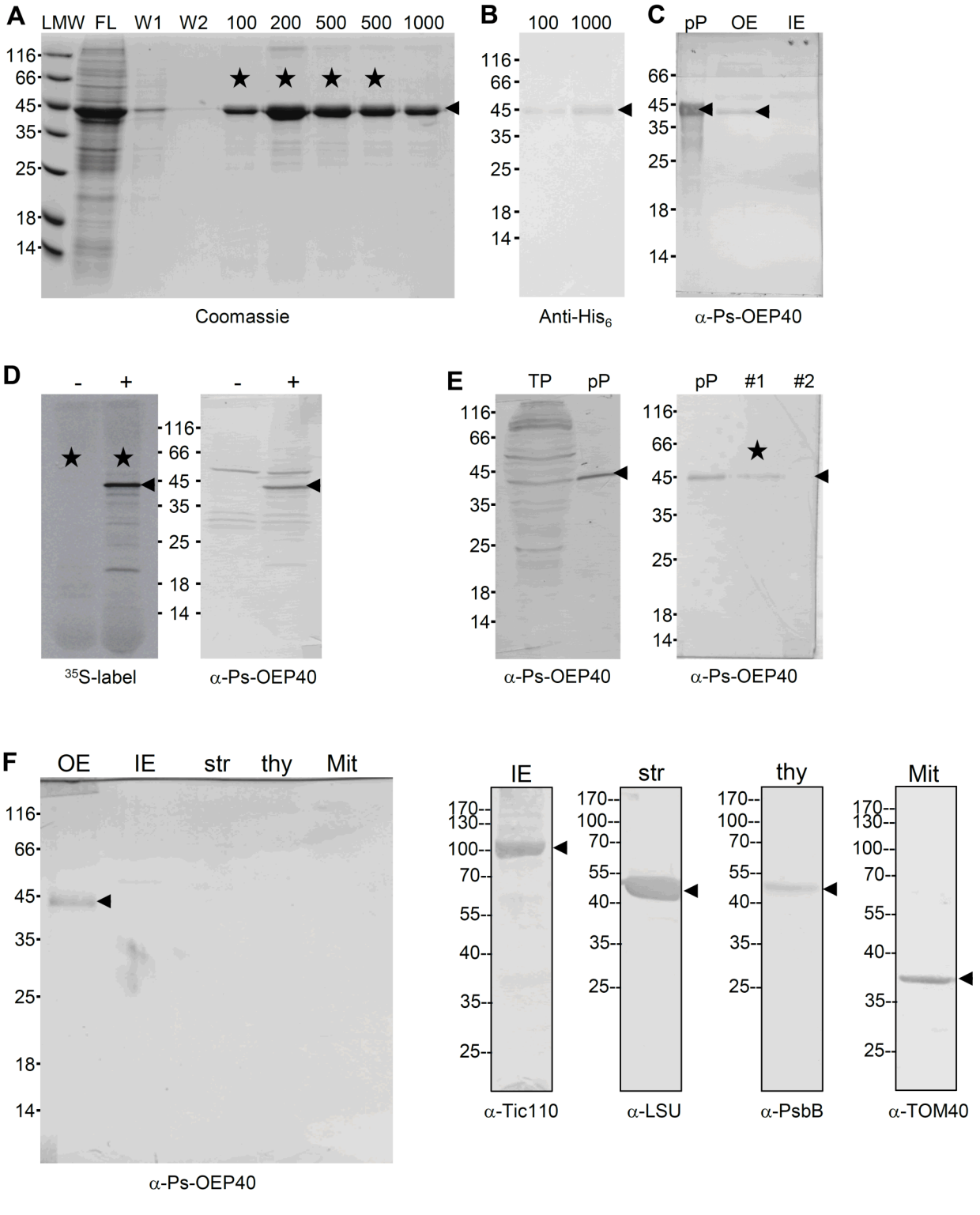
A
LMW FL W1 W2 100 200 500 500 1000
116
66
45
35
25
18
14
Coomassie
B
100 1000
Anti-His6
C
pP OE IE
α-Ps-OEP40
D
- + - +
35S-label
α-Ps-OEP40
E
TP pP
pP #1 #2
α-Ps-OEP40
α-Ps-OEP40
F
OE IE str thy Mit
α-Ps-OEP40
IE
str
thy
Mit
170
130
100
70
55
40
35
25
α-Tic110
α-LSU
α-PsbB
α-TOM40

Figure S2

A

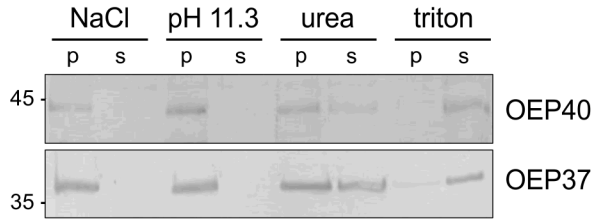

B

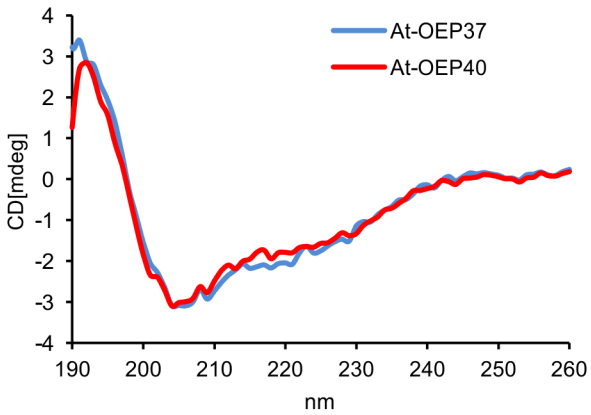

	alpha	beta	turn	unordered
At-OEP40	9.4%	35.6%	20.1%	34.5%
At-OEP37	12.8%	38.2%	19.3%	30.1%

C

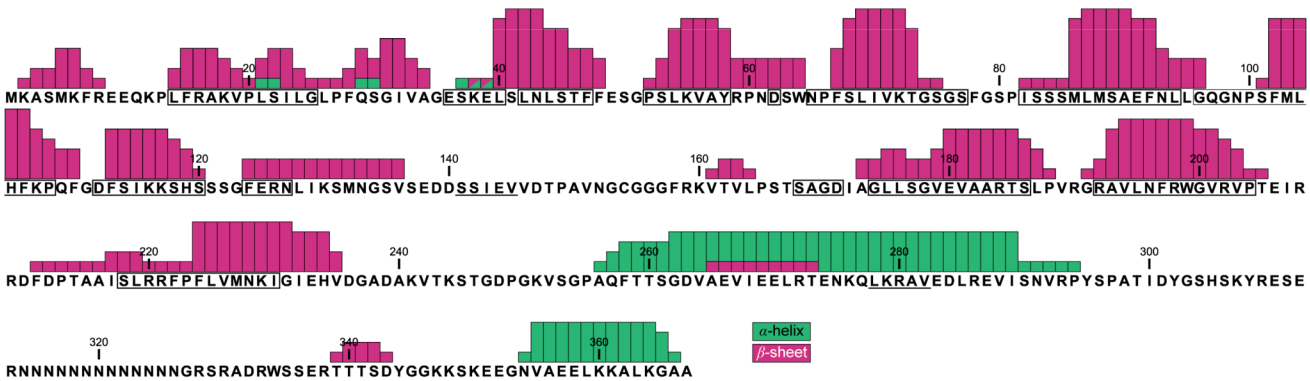

Figure S3

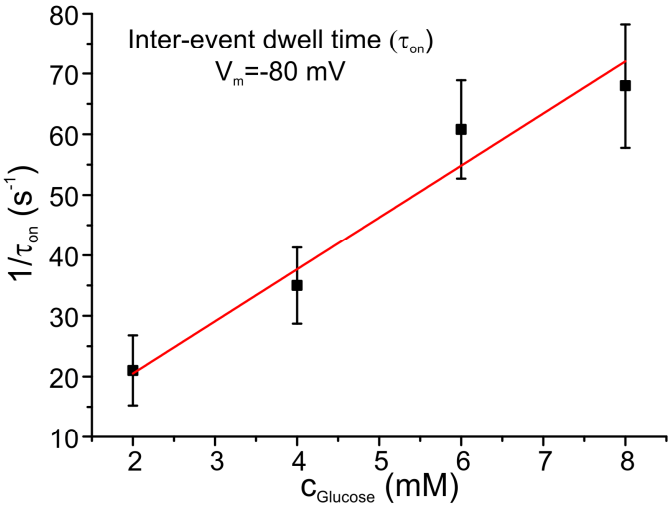
Inter-event dwell time (τ_{on})
V_m=-80 mV
$1/\tau_{on}$ (s^{-1})
$c_{Glucose}$ (mM)
80
70
60
50
40
30
20
10
2
3
4
5
6
7
8

Figure S4

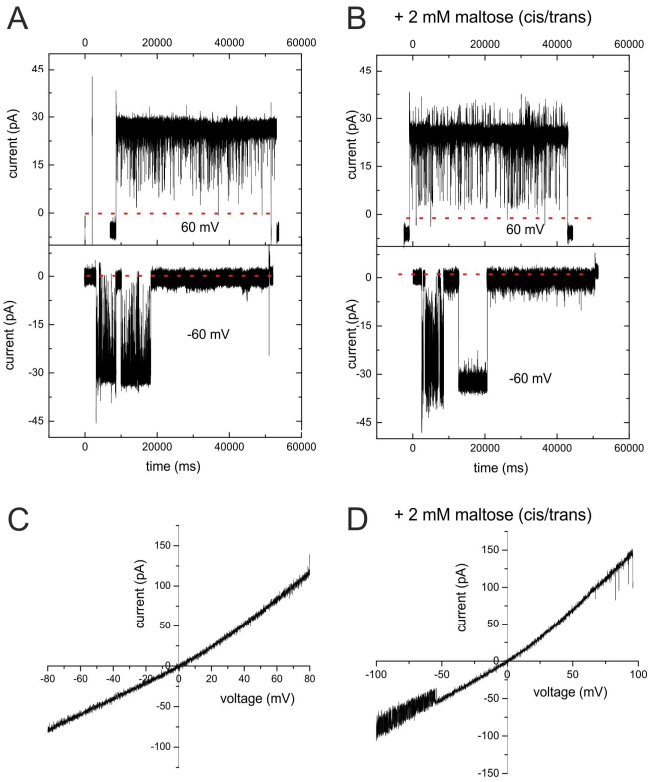
A
B
+ 2 mM maltose (cis/trans)
current (pA)
time (ms)
60 mV
-60 mV
C
D
+ 2 mM maltose (cis/trans)
current (pA)
voltage (mV)

Figure S5

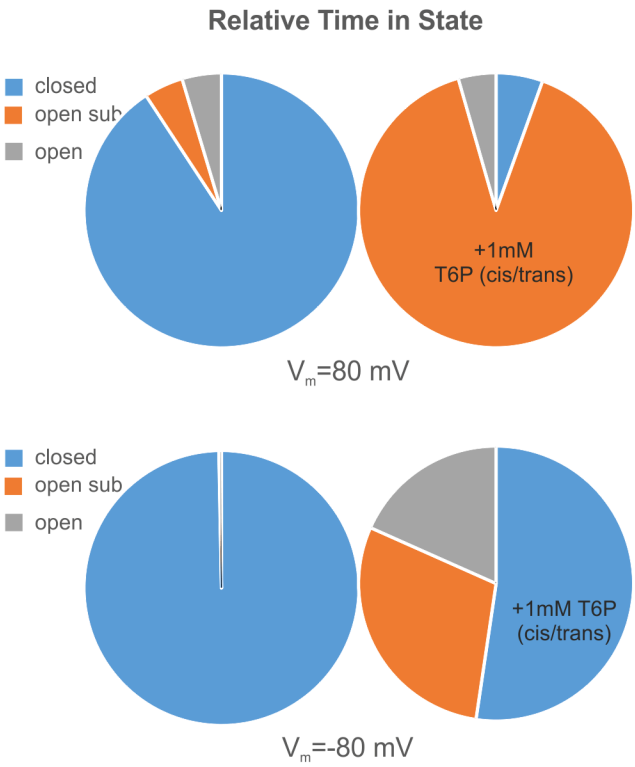
Relative Time in State
closed
open sub
open
+1mM
T6P (cis/trans)
V_m=80 mV
closed
open sub
open
+1mM T6P
(cis/trans)
V_m=-80 mV

Figure S6

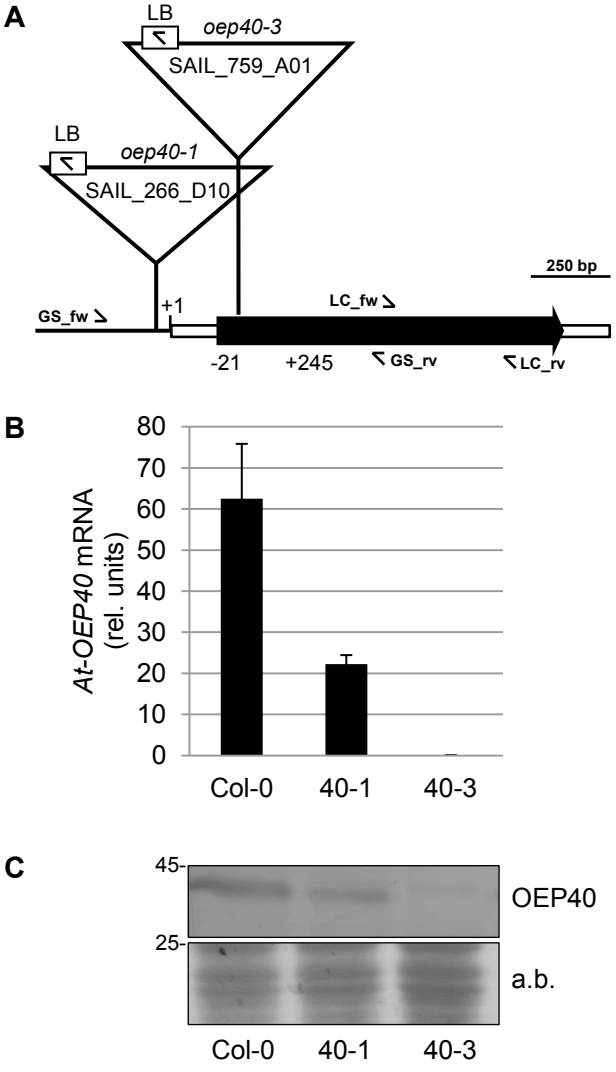
A
LB
oep40-3
SAIL_759_A01
LB
oep40-1
SAIL_266_D10
250 bp
GS_fw
+1
LC_fw
-21
+245
GS_rv
LC_rv
B
At-OEP40 mRNA (rel. units)
80
70
60
50
40
30
20
10
0
Col-0
40-1
40-3
C
45-
25-
OEP40
a.b.
Col-0
40-1
40-3

Figure S7

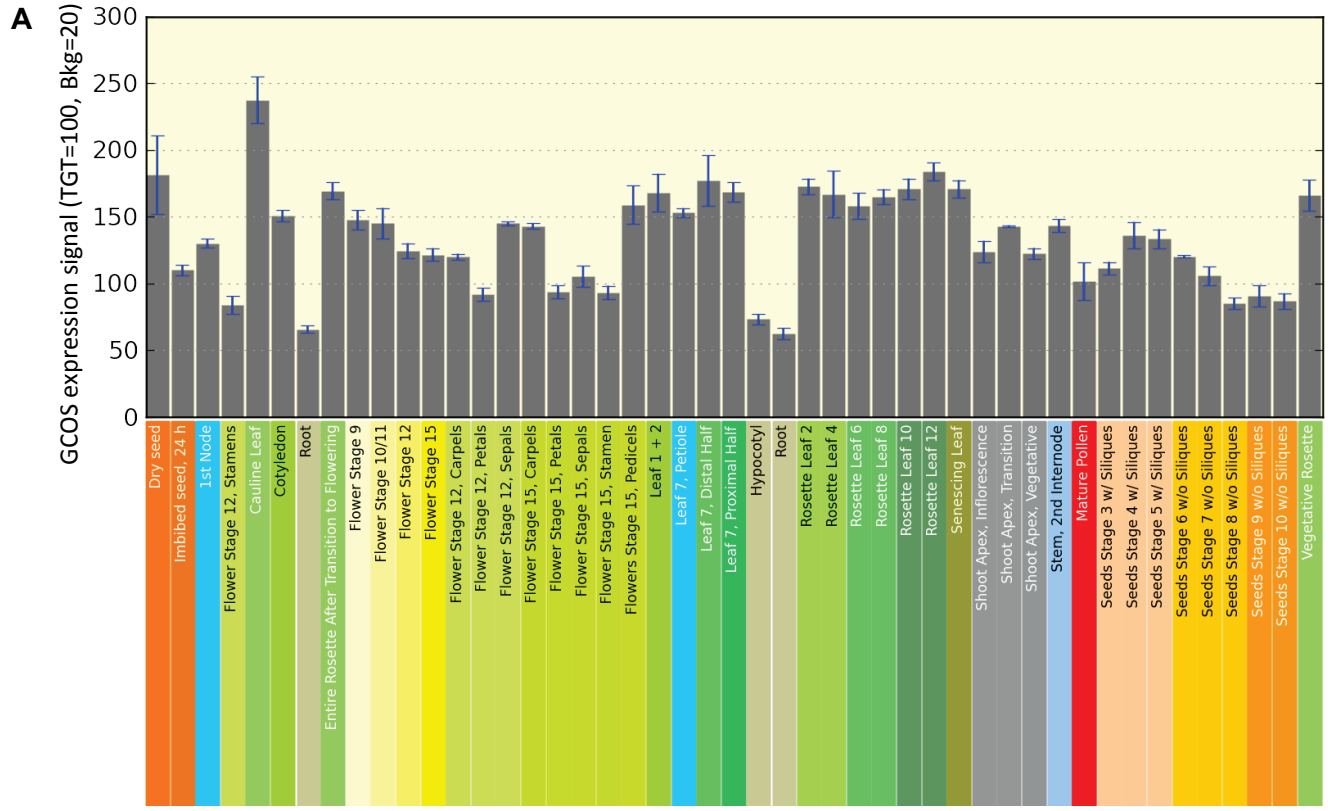
A
GCOS expression signal (TGT=100, Bkg=20)
300
250
200
150
100
50
0
Dry seed
Imbibed seed, 24 h
1st Node
Flower Stage 12, Stamens
Cauline Leaf
Cotyledon
Root
Entire Rosette After Transition to Flowering
Flower Stage 9
Flower Stage 10/11
Flower Stage 12
Flower Stage 15
Flower Stage 12, Carpels
Flower Stage 12, Petals
Flower Stage 12, Sepals
Flower Stage 15, Carpels
Flower Stage 15, Petals
Flower Stage 15, Sepals
Flower Stage 15, Stamen
Flowers Stage 15, Pedicels
Leaf 1 + 2
Leaf 7, Petiole
Leaf 7, Distal Half
Leaf 7, Proximal Half
Hypocotyl
Root
Rosette Leaf 2
Rosette Leaf 4
Rosette Leaf 6
Rosette Leaf 8
Rosette Leaf 10
Rosette Leaf 12
Senescing Leaf
Shoot Apex, Inflorescence
Shoot Apex, Transition
Shoot Apex, Vegetative
Stem, 2nd Internode
Mature Pollen
Seeds Stage 3 w/ Siliques
Seeds Stage 4 w/ Siliques
Seeds Stage 5 w/ Siliques
Seeds Stage 6 w/o Siliques
Seeds Stage 7 w/o Siliques
Seeds Stage 8 w/o Siliques
Seeds Stage 9 w/o Siliques
Seeds Stage 10 w/o Siliques
Vegetative Rosette

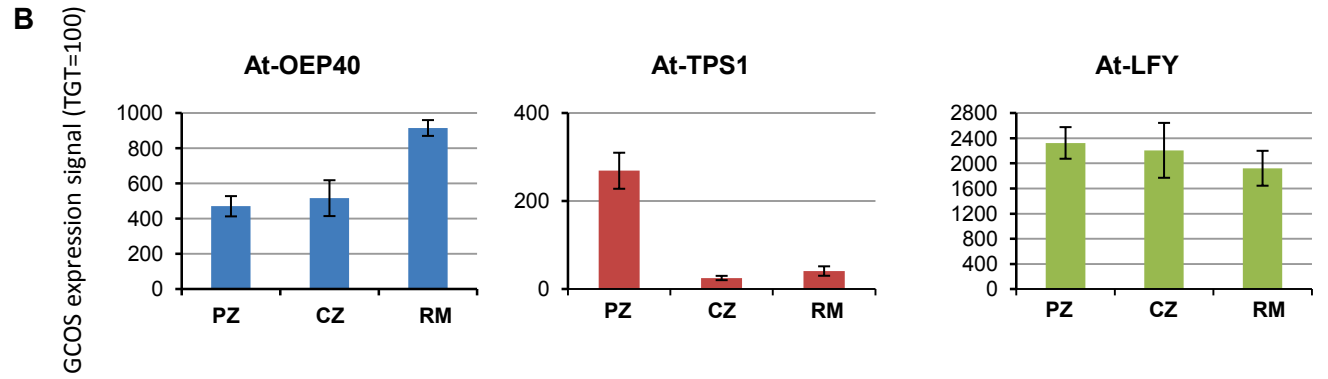
B
GCOS expression signal (TGT=100)
At-OEP40
1000
800
600
400
200
0
PZ
CZ
RM
At-TPS1
400
200
0
PZ
CZ
RM
At-LFY
2800
2400
2000
1600
1200
800
400
0
PZ
CZ
RM

Figure S8